COBEM 2021 26th International Congress of Mechanical Engineering
November 22-26, 2021, Virtual Congress, Brazil

COB-2021-0085
DETERMINATION OF HEATING AND COOLING RATES OF HEAT-AFFECTED ZONE (HAZ) IN LASER WELDING PROCESSES

Ariel Flores Monteiro de Oliveira
Elisan dos Santos Magalhães
Instituto Tecnológico de Aeronáutica – ITA, Divisão de Pós-Graduação e Pesquisa, Praça Mal. Eduardo Gomes, 50 – Vila das Acácias, 12228-900, São José dos Campos, SP, Brazil
arielafmo@ita.br; elisan@ita.br

Luiz Eduardo dos Santos Paes
Universidade Federal de Uberlândia, Uberlândia – MG, Brasil
luiz.paes@ufu.br

Milton Pereira
Universidade Federal de Santa Catarina, Santa Catarina - SC, Brasil
milton.pereira@ufsc.br

Abstract. *Welding technology was originated hundred years ago. Nevertheless, it is still widely used in manufacturing industries as an assembly technique. This procedure has evolved over the years, mostly presenting different types of heat sources. For instance, laser beam welding (LBW) has been widely used in the industry because of its various advantages such as accuracy, low heat flux, and high production rate. Some aspects of the weld beam, including the weld pool size, heat affected zone (HAZ), and microstructure, depend on the heat transfer mechanism and temperature distribution involved in the process. Besides, these aspects are essential to determine welding quality. Therefore, it is vital to understand the characteristics and mechanisms involved in the thermal cycle the welded part is submitted. For that, computational fluid dynamics (CFD) techniques are broadly used since they decrease time and cost compared to experimental procedures. This work presents a study of the heating and cooling rates associated with LBW for the heat-affected zone in autogenous welded steel SAE 1020. This study solved the tridimensional heat diffusion equation considering a moving heat source and the enthalpy function to model the phase change. The equations were solved through the finite volume method (FVM) using an in-house algorithm written in CUDA-C. The numerical software was developed applying SOR-M in the solution of the linear equations since it allows faster processing of data, capable of decreasing up to 30% of processing time and consequently hardware. The welding parameters adopted in the model, such as speed, power, and penetration, were obtained based on the experimental procedure adopted. The experimental and numerical weld bead profile and temperature cycle matched. Therefore, the model is efficient and gives precise estimation that suits practical applications.*

Keywords: *CUDA-C, temperature estimation, heating and cooling rates, laser welding process.*

1. INTRODUCTION

Welding is the earliest method used to assemble parts of materials. This procedure has evolved over the years, existing various processes, manners, heat sources, and types of welds (SAADLAOUI et al., 2018). Nowadays, welding is an essential solution developed for joining parts and materials applied in structures or fuselages (KASHAEV; VENTZKE; ÇAM, 2018).

For instance, laser beam welding (LBW) is a welding process that uses as a heat source a high-energy laser beam generated from solid-state, fiber, laser, or CO_2. The process can be performed autogenously or with additional filler material (KASHAEV; VENTZKE; ÇAM, 2018). This procedure has been widely used in the industry because of its many advantages, such as high welding speed and concentrated heat input (MI et al., 2015). It also induces a high production rate, a small heat-affected zone (HAZ), high energy density (WANG et al., 2020), high joint strength, and process accuracy. Compared to traditional arc welding processes, these factors allow the weld of several complex geometries with low distortion (KASHAEV; VENTZKE; ÇAM, 2018).

The welding input parameters directly affect the welded joint's quality and aspects, including microstructure and mechanical properties (KASHAEV; VENTZKE; ÇAM, 2018). Therefore, monitoring the welded parts allows the investigation and evaluation of how the welding mechanisms and the parameters are related to the weld quality (WANG et al., 2020).

Numerous numerical simulation methods were developed to improve and control the welding process quality (SAADLAOUI et al., 2018). Implementing these methods enables the prediction of many welding factors, namely weld pool geometry, the morphology of microstructure, and even mechanical aspects such as residual stresses. Another essential prediction that can be made by numerical simulation is the thermal cycle. The analysis of phase change and kinetics characterizes the welded joint and predicts the final weld microstructure, which relies on the precise knowledge of the temperature distribution. Besides, it may decrease time and cost in improving experiment procedures (M. SHEHRYAR KHAN, S.I. SHAHABAD, M. YAVUZ, W.W. DULEY, E. BIRO, 2021).

Rosenthal (1946), in his pioneering work, developed an analytic solution considering a moving point source focused on thick and thin sheets to reproduce the surface melt. Since then, numerous works have been published to predict welding attributes. Khan et al. (2021) used numerical modeling to optimize welding quality without decreasing process speed, efficiency, nor productivity by predicting weld pool geometry and the cross-sectional shape of the weld bead, varying the shape and effective spot size on the workpiece. For MI et al. (2015), the primary sources of discrepancy between simulated and experimental results are the non-linear material properties and welding parameters. Their work determined the thermal properties through a linear interpolation of the existent phase fractions in the analyzed steels and the thermal properties for each pure phase. Then, the authors created a three-dimensional finite element code to solve the coupled thermal–metallurgical model. This algorithm forecasted the temperature fields, the volume fraction of phases and predicted its spatial distribution during and after welding. Likewise, Farias, Teixeira, and Vilarinho (2021) used an inverse problem approach and Genetic Algorithms coupled with a Reduced Geometry technique to optimize geometric parameters of heat sources.

This work analyzed the heating and cooling rates associated with the laser welding process for the heat-affected zone in autogenous welded steel SAE 1020. An in-house algorithm written in CUDA-C was used to solve the tridimensional heat diffusion equation, considering a moving heat source and temperature-dependent thermal properties through the finite volume method (FVM). The enthalpy function was applied to model the phase change process. The numerical software was developed applying SOR-M in the solution of the linear equations since it allows faster processing of data, capable of decreasing up to 30% of processing time and consequently hardware cost compared to estimates made without using the platform. Besides, welding parameters such as speed, power, and penetration were obtained based on the experimental procedure adopted. The software was validated by matching the numerically obtained temperature and weld pool geometry results with experimental data.

2. METHODOLOGY

2.1. Mathematical model and simulation:

The first step for modeling the autogenous laser welding process was the mesh definition. In this case, the welded region is small, so the mesh must be well refined. Figure 1 shows how the mesh was defined in the welded pool. Each point corresponds to one volume.

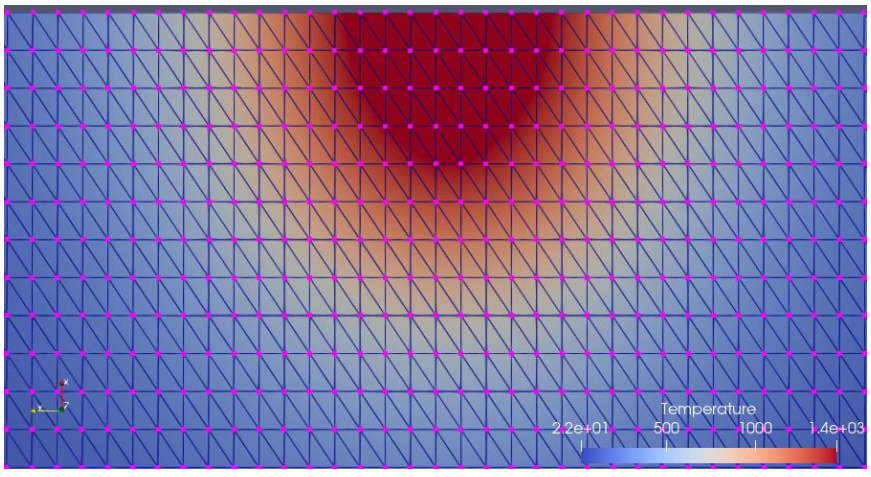

Figure 1: Mesh representation over weld pool region.

The adopted mesh is uniform and constituted by 3.200.000 volumes. The in-house CUDA-C algorithm allows high mesh refinement and does not significantly increase processing time.

The model takes into consideration that the heat transfer is non-linear and occurs in three dimensions. It was also considered a moving heat source, phase change, and temperature-dependent thermophysical properties to predict the temperature distribution during the process and heat loss by convection from the specimen to the shielding gas. Figure 2

shows the relation between thermal conductivity and temperature for SAE 1020 steel (CLAIN; ARAUJO; TEIXEIRA, 2017).

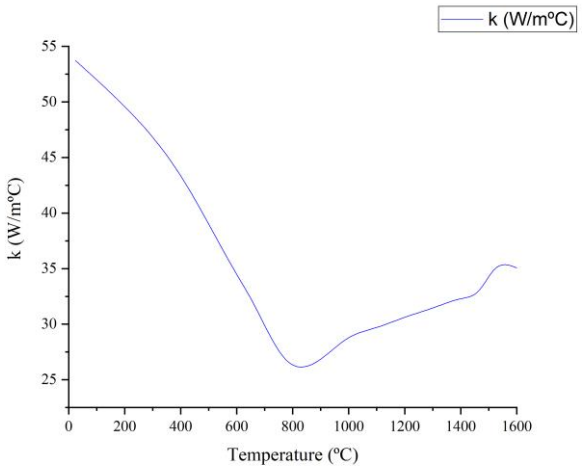

Figure 2. Thermal conductivity of SAE 1020 steel.

The equations solutions were obtained through the finite volume method. Furthermore, the following heat diffusion equation allows the acquisition of the temperature field for the solid region.

$$\frac{\partial}{\partial x}\left(k(T)\frac{\partial T}{\partial x}\right)+\frac{\partial}{\partial y}\left(k(T)\frac{\partial T}{\partial y}\right)+\frac{\partial}{\partial z}\left(k(T)\frac{\partial T}{\partial z}\right)=\frac{\partial H(T)}{\partial t} \tag{1}$$

where k is the thermal conductivity, T is the temperature, and H is the enthalpy function.

As shown in Eq. (1), the tridimensional heat diffusion equation is based on the enthalpy function described by:

$$H(T)=\int_{T_0}^{T}\left[\rho(\theta)c(\theta)+\rho(\theta)L\delta(\theta-T_m)\right]d\theta \tag{2}$$

where T is the temperature T_0, and T_m is the reference and fusion temperatures, respectively, c is the specific heat, and L is the latent heat of solidification. Note that the specific heat is a function of the temperature and its values firmly depend on it.

Some boundary conditions were set since the sheet is subjected to convection and radiation, as:

$$-k(T)\frac{\partial T}{\partial \eta_i}=h(T)\left(T-T_\infty\right)+\sigma\varepsilon(T)\left(T^4-T_\infty^4\right) \tag{3}$$

where T is the calculated temperature, η_i are the normal surfaces, i stands for the number of flat surfaces, h is the convection heat transfer coefficient, σ is the Stefan–Boltzmann constant, ε is the emissivity, and T_∞ is the room temperature.

The heat loss by convection suffered by the sides of the sheet can be calculated by the free convection model developed by INCROPERA et al. (2008), as:

$$Nu_x=\frac{hx}{k}=-\left(\frac{Gr_x}{4}\right)^{\frac{1}{4}}\left.\frac{dT^*}{d\eta}\right|_{\eta=0}=\left(\frac{Gr_x}{4}\right)^{\frac{1}{4}}g(\mathrm{Pr}) \tag{4}$$

where Nu, Gr, and Pr are the Nusselt, Grashof, and Prandtl numbers, respectively.

The experimental radius and penetration of the weld bead were obtained by micrograph analysis, while the dimensions obtained numerically were measured using the analytical software Paraview.

2.2 Experimental procedure:

The SAE 1020 steel sheets were autogenously welded employing a fiber laser power source IPG-YLS 10000, creating a weld bead of 45mm. The maximum power output of the laser was 3kW, and the beam was placed, resulting in an 880 µm focal diameter over the specimen, with Gaussian distribution. The welding speed was set at 0.05 m/s. An argon flow of 15 l/min was used as a shielding gas to prevent reactions with the atmosphere. The experiments were repeated three times.

The thermal data was acquired from a National USB 6218 board with 32 inputs, 16 bits, and 250 kb/s. The acquisition rate was 10 Hz. As shown in Figure 3, nine type k thermocouples were equidistantly attached along the x-axis, and 2mm over the center of the sheet, the distance between the thermocouples was 5mm.

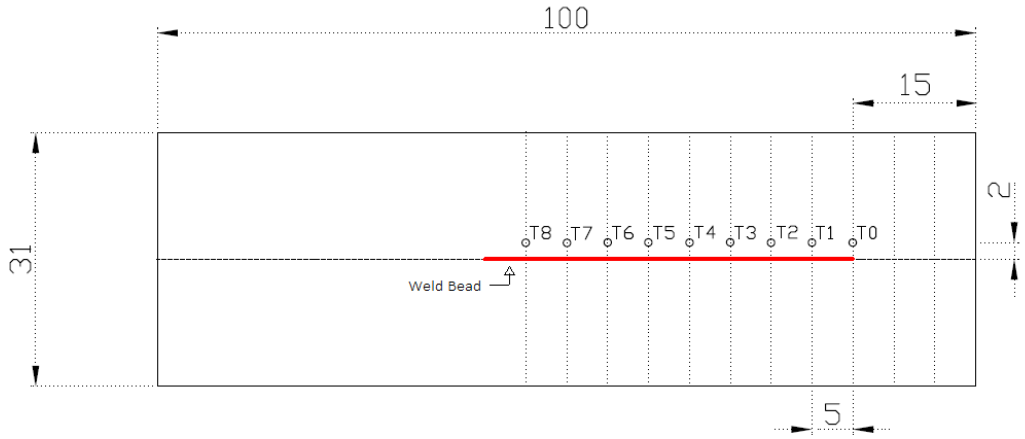

Figure 3. Schematic representation of thermocouples fixation, measures in millimeters.

3. RESULTS

The dimensions of the experimental weld bead were obtained by micrograph analysis, as shown in Figure 4.

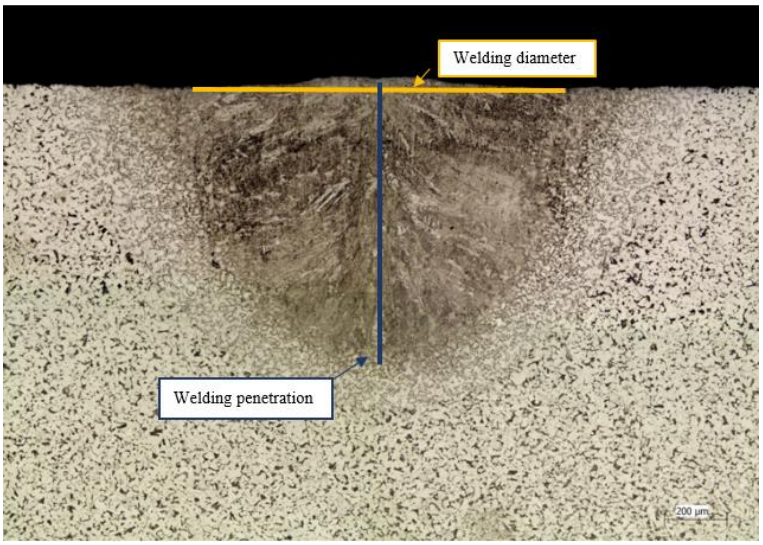

Figure 4. Cross-section micrograph of SAE 1020 autogenously welded.

The dimensions of the numerical weld bead were acquired using Paraview. Figure 5 shows the cross-section of the weld bead, colored by temperature. Note that the axes orientation is unique to the software and does not correspond to the orientation adopted in the code.

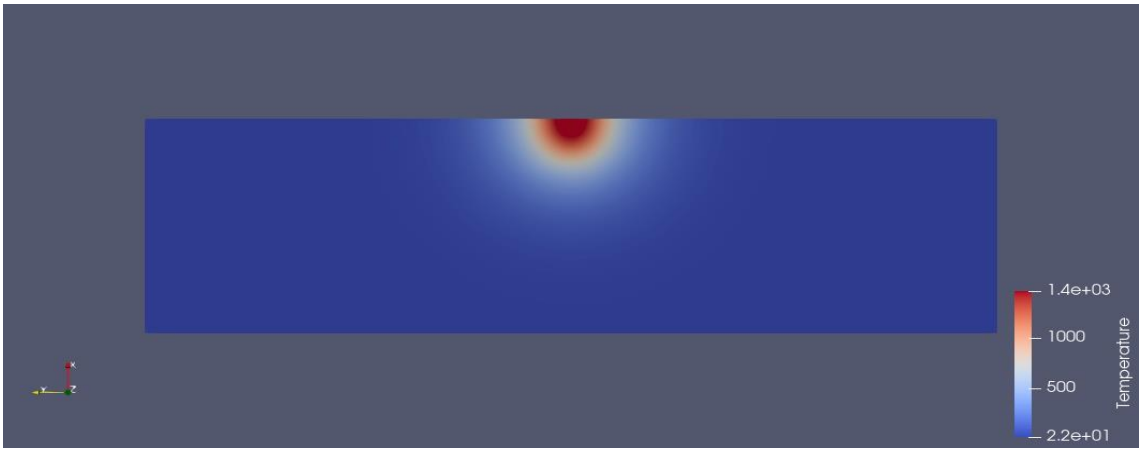

Figure 5. Cross-section scheme of the numerical weld bead.

Both experimental and numerical dimensions are expressed in Table 1.

Table 1. Experimental and numerical weld bead dimensions.

	Welding Radius (m)	**Welding Penetration (m)**
Experimental	0.000600	0.000842
Numerical	0.000605	0.000843
Dimension difference ($m \times 10^{-6}$)	5	1
Standard deviation ($m \times 10^{-6}$)	3.53553	0.707107

As shown, there is no significant difference nor standard deviation between the experimental and numerical sizes. Thus, the algorithm succeeded in the prediction of the weld pool shape.

The experimental and numerical temperature fields were also compared. The room temperature during the experiment was 22ºC. This temperature was set in the code. Both experimental and numerical thermal cycles are shown in Figures 6 and 7, respectively.

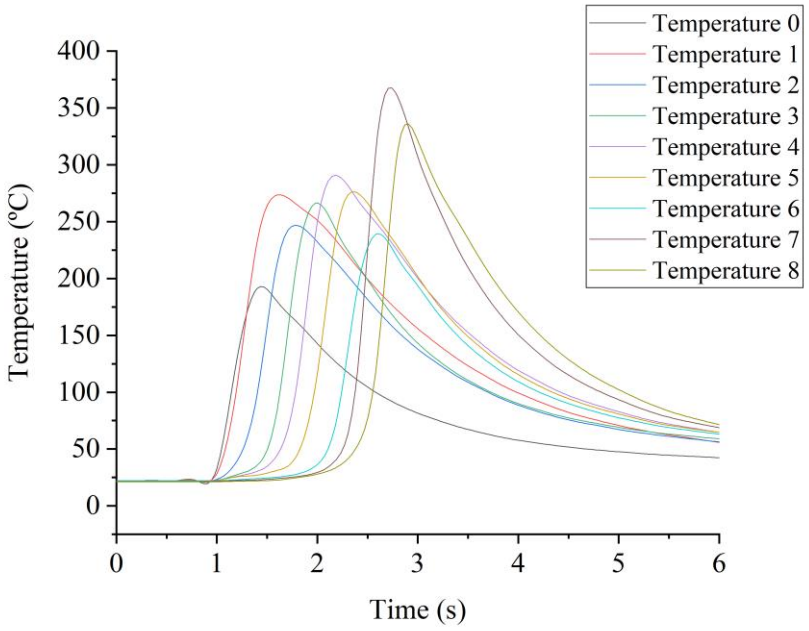

Figure 6. Experimental thermal welding cycle.

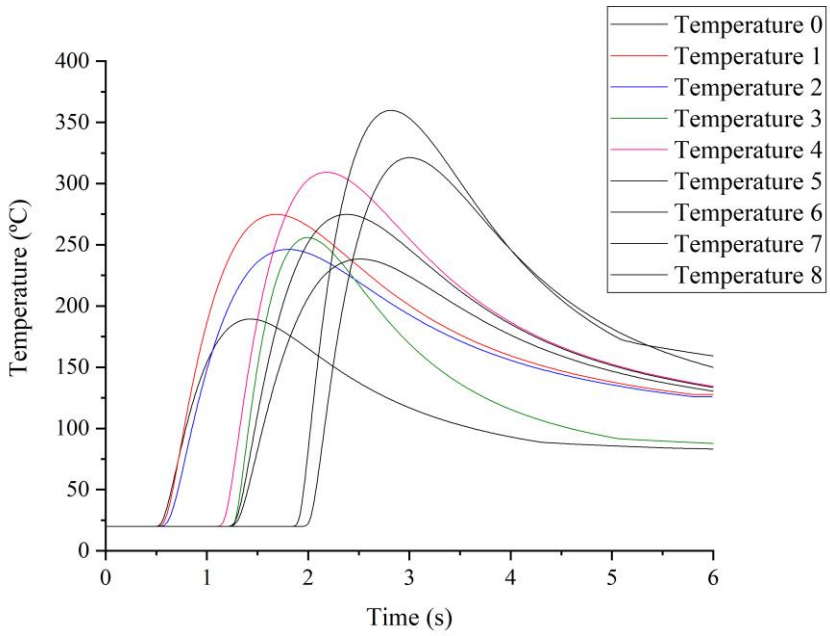

Figure 7. Numerical thermal welding cycle.

As shown in Figures 6 and 7, both cycles presented similar behavior. For every position along with the weld bead, the temperature increases from room temperature until it reaches peak temperature within the first seconds and decreases at the end of the cycle. If the results were projected in time, the sample temperature would decrease until room temperature due to heat loss from the sample to the surroundings.

Besides room temperature is the same for all sensors, each one acquired a different peak temperature, as presented in Table 2.

Table 2. Experimental and numerical peak temperatures.

	Peak temperature (ºC)		**Error percentage (%)**
	Experimental	**Numerical**	
Temperature 0	191.14	189.35	0.94
Temperature 1	273.54	274.85	-0.48
Temperature 2	246.70	246.25	0.18
Temperature 3	266.50	255.89	3.98
Temperature 4	290.46	309.21	-6.45
Temperature 5	275.34	274.85	0.18
Temperature 6	239.47	238.41	0.44
Temperature 7	359.94	359.79	0.04
Temperature 8	321.37	321.21	0.05

The numerically obtained temperatures resemble the experimental data, with deviations from 0.1520ºC (Temperature 7) to 18.7454 ºC (Temperature 4). Negative percentage values are found when numerical peak temperature is higher than experimental. Furthermore, the error percentage modulus is less than 1 for the majority of measures.

The temperature differences are mainly due to experimental errors induced by sensors and their attachment to the workpiece. Moreover, the distance between the sensors and the weld bead can also induce errors. Indeed, the temperature strongly depends on the analyzed position both for the experiment and the algorithm.

4. CONCLUSIONS

A numerical model was developed to study the thermal cycle involved in the LBW process. The algorithm was used to solve the heat diffusion equation through the FVM, considering some process' aspects such as a moving heat source, temperature-dependent thermal properties, phase change, boundary conditions, and heat loss by convection.

The code validation was made by comparison with experimental results. The code acquired precise results for the weld pool geometry with differences of 5 and 1 micrometers for the welding radius and penetration, respectively.
Another essential condition for code validation is to match the temperature profile. As shown in Fig. 6 e Fig 7. the numerically obtained cycle is similar to the experimental one. During the weld, the sample is initially at room temperature and heats until temperature reaches a maximum, succeeded by cooling.

Also, there are no significant deviations from the numerical and experimental temperature values, as shown in Table 2. The deviations occur due to experimental errors induced by the sensors' attachment to the sample and the distance between sensors and weld bead. Indeed, the temperature strongly depends on the analyzed position for both experiment and algorithm.

Therefore, both weld pool geometry and thermal cycle predicted by the code were accurate. Hence, the algorithm can be used to predict these weld parameters successfully.

5. ACKNOWLEDGEMENTS

The authors would also like to acknowledge the Aeronautics Institute of Technology, Federal University of Uberlândia, and CAPES for the opportunity and financial support.

6. REFERENCES

CLAIN, F.; ARAUJO, D.; TEIXEIRA, P. a Heat Source Model To Simulate Welding Processes With Magnetic Deflection. v. 22, n. 1, p. 99–113, 2017.
FARIAS, R. M.; TEIXEIRA, P. R. F.; VILARINHO, L. O. An efficient computational approach for heat source optimization in numerical simulations of arc welding processes. **Journal of Constructional Steel Research**, v. 176, p. 106382, 2021.
INCROPERA, F. P. et al. **Fundamentos de transferência de calor e massa**. [s.l: s.n.].
KASHAEV, N.; VENTZKE, V.; ÇAM, G. Prospects of laser beam welding and friction stir welding processes for aluminum airframe structural applications. **Journal of Manufacturing Processes**, v. 36, p. 571–600, 1 dez. 2018.
M. SHEHRYAR KHAN, S.I. SHAHABAD, M. YAVUZ, W.W. DULEY, E. BIRO, Y. Z. Numerical modelling and experimental validation of the effect of laser beam defocusing on process optimization during fiber laser welding of automotive press-hardened steels | Elsevier Enhanced Reader. **2021**, p. 535–544, 2021.
MI, G. et al. A thermal-metallurgical model of laser beam welding simulation for carbon steels. **Modelling and Simulation in Materials Science and Engineering**, v. 23, n. 3, 2015.
SAADLAOUI, Y. et al. A new strategy for the numerical modeling of a weld pool. **Comptes Rendus - Mecanique**, v. 346, n. 11, p. 999–1017, 2018.
WANG, L. et al. Monitoring of keyhole entrance and molten pool with quality analysis during adjustable ring mode laser welding. **Applied Optics**, v. 59, n. 6, p. 1576, 2020.

7. RESPONSIBILITY NOTICE

The authors are the only ones responsible for the printed material included in this paper.